Int. J. Electrochem. Sci., 16 **(2021)** Article ID: 210945, doi: 10.20964/2021.09.09

International Journal of ELECTROCHEMICAL SCIENCE
www.electrochemsci.org

Improving the Photocatalytic Properties of TiO_2 Coatings by Modification of the Pore Size and the Crystalline Structure by Combining Anodization and MAO Technology

Song Wei[*,#]*, Xie Ying-Nan*[#]*, Wang Yi-Long, Huang Xi-Tong, Wang Xiao-Lei*

School of Biological and Chemical Engineering, Nanyang Institute of Technology. NO.80 Changjiang Road, Nanyang, He'nan, 473004, China
#SONG Wei and #XIE Ying-nan contributed equally to this work.
[*]E-mail: song78wei@163.com

Received: 30 April 2021 / *Accepted:* 18 June 2021 / *Published:* 10 August 2021

A TiO_2 coating with regular pore parameters was fabricated on the surface of pure titanium metal. The pore size and crystalline structure of the coating were modified by combining anodizing and micro arc oxidation technology. The cross-section and micro-surface of the anodic coating were observed by SEM, which suggested that the pore size of the anodic coating can be adjusted to 81 nm by using sulfuric-phosphoric acid as the electrolyte. The micro-surface of the coatings was characterized by SEM after MAO treatment, and ImageJ software was used to study the porosity of the coating. The results proved that when the current density was 30 mA/cm^2, the porosity of the coating was 20.12 %, and few microcracks were found on the surface of the coating. The crystalline structure of the coating was studied by XRD, and the results proved that anatase can be transformed into a rutile crystalline structure by MAO technology. The absorbance of the coating was tested and compared with that of TiO_2 powder by UV-vis spectroscopy; the results proved that the absorption wavelength range of the coating became wider after it had been treated by anodizing and MAO technology. The activity and stability of the photocatalyst was studied by measuring the absorbance of a methyl orange solution before and after treatment with the coating, and the results proved that the coating had better activity in the degradation of methyl orange. After the photocatalyst had been used 5 times, the specific activity of the coating exceeded 85 % of that of the new photocatalyst.

Keywords: TiO_2 coating; photocatalyst; anodizing; micro arc oxidation; pore size; crystalline structure

1. INTRODUCTION

Every year, billions of tons of municipal wastewater and industrial water are discharged to sewers, rivers, lakes, and the sea every year. Therefore, there is an increasing demand for more efficient and economic wastewater treatment technology to remove recalcitrant compounds, including pollutants of emerging concern[1]. TiO_2 is non-toxic and chemically stable, it has a low-cost, optical, electronic

and physiochemical properties[2], and it has become a multifunctional material with a wide variety of potential applications, including solar cells[3], photocatalysts[4][5][6], water splitting[7], and gas sensors[8]. Homogeneous[9] and heterogeneous[10] photocatalytic oxidation is useful for oxidizing nonbiodegradable compounds. The principles and kinetic models of these reactions are described in the literature[11][12][13]. Many plants have been set up to treat industrial wastewater with powdered TiO_2 (P25) as a photocatalyst[14][15]. However, it is difficult to separate wastewater and powdered photocatalysts. In addition, it is difficult to design continuous water treatment processes that use nanocrystalline TiO_2 suspensions in fluidized bed reactors due to the necessary separation step when the water exits the reactor. Another disadvantage of TiO_2 suspensions is the scattering of incident light that occurs on small TiO_2 particles, which leads to high attenuation of light energy and consequently small penetration depths. TiO_2 has three crystalline structures: rutile (stable), anatase (metastable) and brookite (metastable). Although there is a debate in the literature, the common opinion is that when the photocatalyst has a crystalline composition of 75 wt % anatase and 25 wt % rutile, it has higher photocatalytic activity. The wide bandgap of TiO_2 (3.2 eV for the anatase phase and 3.0 eV for the rutile phase) requires ultraviolet (UV) light for electron-hole separation, which makes up only 5 % of natural solar light. It is of great significance to develop photocatalysts that can be used in both UV and visible light irradiation to improve photocatalytic efficiency. To improve the photocatalyst efficiency of TiO_2, in the last few years, TiO_2 has been doped with various alkaline earth metal ions (Ca^{2+}, Sr^{2+}, Ba^{2+})[16][17], transition metal ions (Fe^{3+}, Cr^{6+}, Co^{3+}, Mo^{5+})[18][19], and rare earth cations (La^{3+}, Ce^{3+}, Er^{3+}, Pr^{3+}, Gd^{3+}, Nd^{3+}, Sm^{3+})[20][21] induce a redshift by decreasing the bandgap or introducing band gap states. Although this approach was able to reduce the bandgap of TiO_2, it suffers from the presence of a carrier recombination centre and the formation of strongly localized states within the band gap, which significantly reduce carrier mobility.

Powdered TiO_2 has been immobilized in films to simplify the separation process. In addition, it has been reported that using nonmetal ions (C, N, F, and S)[22][23] is more appropriate for extending the photocatalytic activity of TiO_2 into the visible region than metal cation-doped catalysts. At present, TiO_2 nanotubes (TNTs) display high-performance levels for their potential in improving photocatalytic activity because of their large surface area. There are many methods of preparing heterogeneous immobilized catalysts, such as those immobilized on TiO_2 nanotubes; these methods include anodizing[24], MAO[25], CVD[26], PVD[27], sol-gel[28], liquid deposition[29] and magnetron sputter[30] technologies. Among the simplest, cheapest, and most straightforward approaches that lead to ordered nanostructures of TiO_2 are anodizing and MAO techniques, which can be used to prepare highly ordered porous TiO_2 coatings on the surface of titanium or its alloys. Additionally, the photocatalytic activity of TiO_2 nanotubes is related to their size, specific surface area, and preparation technology[31]. TiO_2 coatings with ordered pore parameters can be obtained on the surface of titanium metal or its alloys by anodizing technology; however, the crystalline composition of the anodic coating is amorphous and anatase. Although the coating composition can be transformed into rutile at a high temperature of 400-500 ℃ via hydrothermal treatment, the adhesion between the coating and substrate is low, and the stability of the photocatalyst is limited[32]. TiO_2 with a rutile crystalline structure can be obtained on the surface of titanium metal or its alloys by MAO technology. During MAO, a rutile TiO_2 coating with good adhesion and a smooth surface can be obtained[33]. However, the crystalline structure

of the coating mainly consists of rutile, and the photocatalytic activity is low. In addition, the coating has many microcracks[34], which decrease the specific surface area of the coating.

If anodizing and MAO technology are combined, a titanium oxide coating can be prepared on the surface of titanium metal or its alloys. The pore size and pore distance of the anodized coating can be modified easily. Then, amorphous and anatase titanium oxide can be transformed into rutile through MAO. To improve the photocatalytic activity of the TiO_2 coating, based on the composition of P25, the composition of the coating should be 75 % anatase and 25 % rutile. The transformation rate of amorphous and anatase TiO_2 can be regulated by adjusting the energy density, which is determined by supply power parameters. For a pulse supply power, many parameters affect the plasma discharge. Among them, the current density directly affects plasma discharge. Thus, in our research, the influence of current density on the transformation of amorphous anatase into rutile was studied by X-ray diffraction. The microstructure of the coating was observed by scanning electron microscopy, the porosity of the coating was analysed by ImageJ software, the absorbance wavelength of the photocatalyst was measured by UV-vis spectrophotometry, and the photocatalytic activity and stability of the coating were studied by determining the absorbance of methyl orange solution before and after photocatalytic treatment.

2. EXPERIMENTAL

2.1 The preparation of catalyst TiO_2/Ti.

Each of our experimental reagents was provided by Tianjin Kemiou Chemical Reagent Co. Ltd. Commercially pure titanium ($20 \times 20 \times 1$ mm^3) was used as the specimen, and the anodizing procedure was conducted with a stirring speed of 60 r/min and a current density of 50 mA/cm^2 at 4 ℃ for 40 min. Thereafter, the coatings subjected to anodizing treatment were prepared with electrolytes consisting of sulfuric (110 g/L) and phosphoric acids with concentrations of 0, 9.5, 19, and 28.5 g/L. When the anodic coatings reached 50 μm, each specimen was rinsed with deionized water before immersion within the stirred electrolyte containing 15 g/L Na_2SiO_3, 5 g/L $(NaPO_3)_6$, and 5 g/L KOH. The MAO procedure was conducted with a duty cycle of 10 % and a pulse frequency of 20 kHz for 15 min at current densities of 10 mA/cm^2, 30 mA/cm^2, and 50 mA/cm^2.

2.2 Characterization and photocatalytic performance test

An X-ray diffractometer (XRD; D/max-RB, RICOH, Japan) containing CuKa sources was employed to examine the phase compositions of different coatings. The accelerating voltage and applied current were 40 kV and 30 mA, respectively. Scanning electron microscopy (SEM; S-4700, Hitachi, Japan) was adopted to investigate the coating's cross-sectional microstructure and surface microstructure. The porosity and the average pore size of the coatings were statistically analysed by ImageJ software.

Methylene orange (MO) solutions were prepared with distilled water without pH adjustment. The absorbance of a stock solution of MO at concentrations of 10 mg/L, 20 mg/L, 30 mg/L and 40 mg/L

was determined by UV-vis spectroscopy (HACH, DR 5000). Scans were performed in the range of 200 to 700 nm and at a scan rate of 1 nm/s^{-1}. Formula (1) was applied to determine the absorbance before and after the photocatalytic treatment.

$$A=\lg(I_t/I_0) \quad (1)$$

In formula (1), A represents the absorbance, I_t represents the transmitted light intensity, and I_0 represents the incident light intensity. According to formula (2), the catalytic activity of TiO_2 is determined by the degradation rate of MO.

$$\eta = \frac{(C_0 - C_t)}{C_0} \times 100\% = \frac{(A_0 - A_t}{A_0} \times 100\% \quad (2)$$

In formula (2), η represents the degradation rate of MO (%), C_0 and C_t represent the MO concentration (mg/L) before and after photocatalytic degradation, respectively, and A_0 and A_t represent the absorbance of the MO before and after treatment.

3. RESULTS AND DISCUSSION

3.1 Pore size of the anodic coatings

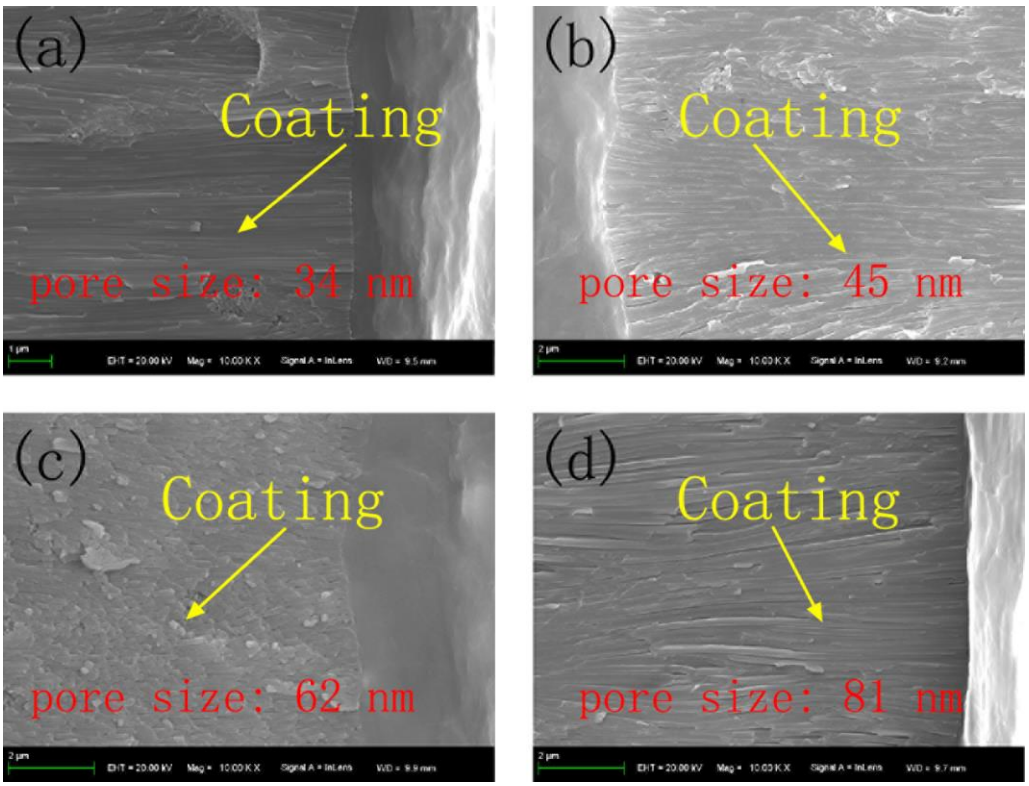

Figure 1. Pore size of the anodic coating at a sulfuric acid concentration of 110 g/L and a current density of 50 mA/cm^2 at 4 °C for 40 min; phosphoric acid concentration of (a) 0 g/L; (b) 9.5 g/L; (c) 19 g/L and (d) 28.5 g/L, respectively

Enlarging the pore size of the coating favours the transfer of degradation products in and out of the pore, but it decreases the specific surface area. To degrade the polymer, a suitable pore size should not be smaller than 70 nm. The pore size of the TiO_2 coating obtained in sulfuric acid is approximately 20-40 nm, while that in phosphorous acid is approximately 500 nm[35]. To adjust the pore size of the TiO_2 coating, sulfuric-phosphoric acid was mixed as the electrolyte, and the influence of the phosphoric acid concentration on the pore size of the anodic coating was studied and is illustrated in Fig. 1. Fig. 1 shows that with the increase in phosphoric acid concentration from 0 g/L to 28.5 g/L, the pore size of the TiO_2 coating increased from 34 nm to 81 nm. These data were consistent with the expected pore size of the photocatalyst.

To further analyse the microstructure of the anodic TiO_2 coating, its micro-surface morphology was observed by SEM, and its porosity was analysed by ImageJ software. The results are shown in Fig. 2 and Fig. 3, respectively.

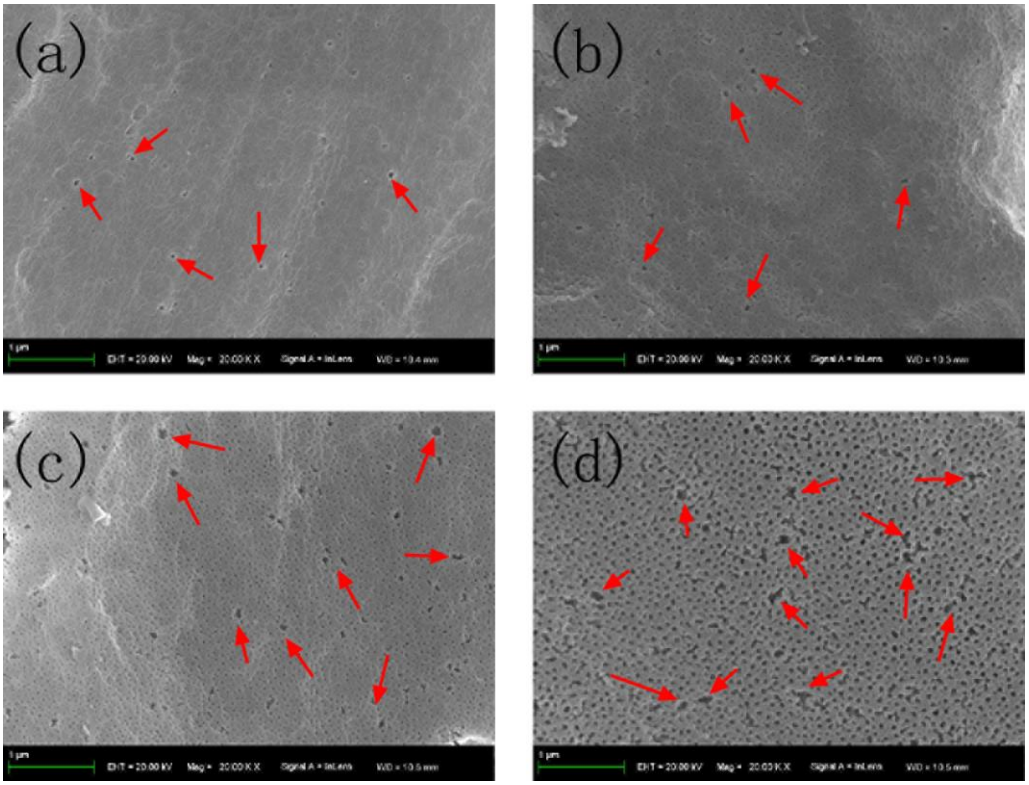

Figure 2. Micro-surface morphology of the anodic coating at a sulfuric acid concentration of 110 g/L and a current density of 50 mA/cm^2 at 4 ℃ for 40 min. Phosphoric acid concentrations of (a) 0 g/L, (b) 9.5 g/L, (c) 19 g/L and (d) 28.5 g/L.

Fig. 2 shows that with increasing phosphoric acid concentration, the pore size of the coating increased[36]. The results confirmed the conclusion drawn from Fig. 1. In addition, with increasing pore size, the pore distance increased while the pore quantity decreased. Additionally, the distribution of the pore sizes became inhomogeneous, and the quantity of inhomogeneous pores increased. The active sites

of the catalyst were related to the specific surface area of the coating, and the specific surface area of the coating decreased with increasing pore size and pore distance. Therefore, the phosphoric acid concentration should not be higher than 28.5 g/L.

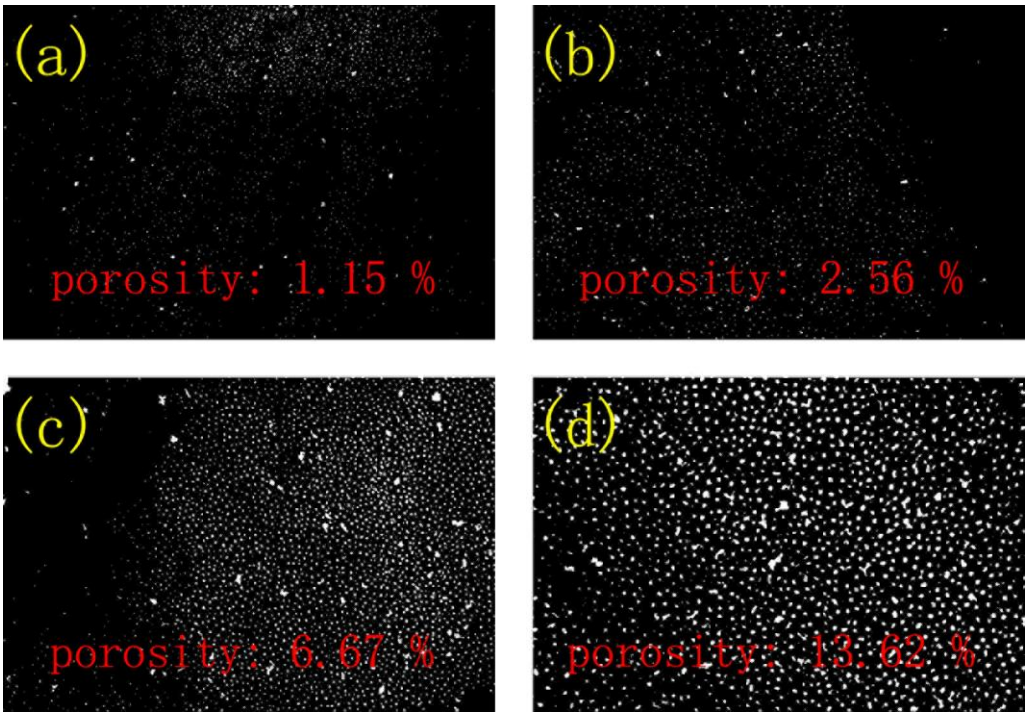

Figure 3. Porosity of the anodic coating at a sulfuric acid concentration of 110 g/L and a current density of 50 mA/cm^2 at 4 ℃ for 40 min. Phosphoric acid concentrations of (a) 0 g/L; (b) 9.5 g/L; (c) 19 g/L and (d) 28.5 g/L.

The porosity of the coating was analysed by ImageJ software. With increasing phosphoric acid concentration, the porosity of the coating increased, and holes with homogeneous pore sizes were evenly distributed in the coating, which was beneficial for improving the photocatalytic activity of the TiO_2 coating.

3.2 Crystallization of the coatings

During MAO, as the plasma discharged, the in situ temperature could reach 10^3-10^4 K. Due to the high temperature generated by the plasma discharge, the Ti metal was melted and ejected into the coating. Thus, there were characteristic peaks of Ti metal in the XRD patterns. The anatase in the anodic TiO_2 coating could be transformed into rutile TiO_2. The crystalline structure of the coating can be adjusted by this method. The XRD patterns of the anodic coating before and after treatment by MAO technology at current densities of 10, 30, and 50 mA/cm^2 were obtained, and the results are shown in Fig. 4.

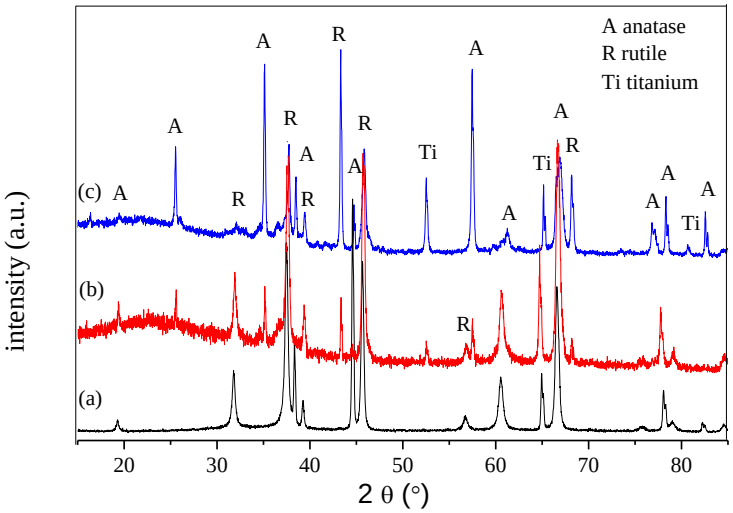

Figure 4. X-ray diffraction (XRD) patterns of (a) anodic TiO_2 treated by MAO technology in electrolytes containing 15 g/L Na_2SiO_3, 5 g/L $(NaPO_3)_6$, and 5 g/L KOH. The MAO procedure was conducted with a duty cycle of 10 %, a pulse frequency of 20 kHz for 15 min and a current density of (b) 10 mA/cm^2 and (c) 50 mA/cm^2.

Fig. 4 shows that the anodic TiO_2 coating had anatase, which was consistent with the conclusion of a prior study[37]. After MAO treatment, characteristic anatase, rutile, and titanium peaks appeared in the XRD pattern, which proved that anatase TiO_2 could be transformed into rutile TiO_2[38]. In addition, with increasing current density, the intensity of rutile and titanium characteristic peaks increased, proving that the crystalline transformation of anatase increased with increasing current density. According to the crystalline composition of P25, the suitable anatase and rutile ratio is 75:25; thus, crystalline transformation should be carried out at a lower current density.

3.3 Porosity of the coatings

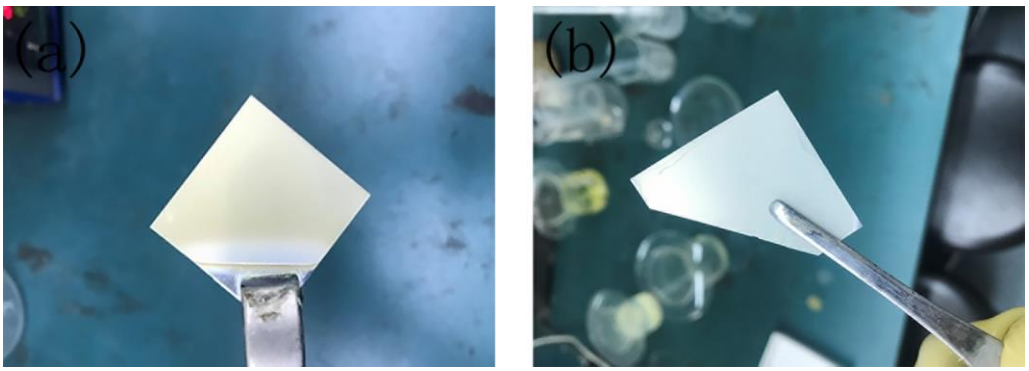

Figure 5. Photograph of the anodic TiO_2 coating before and after MAO treatment in an electrolyte containing 15 g/L Na_2SiO_3, 5 g/L $(NaPO_3)_6$, and 5 g/L KOH. The MAO procedure was conducted with a duty cycle of 10 %, a pulse frequency of 20 kHz for 15 min and a current density of (b) 10 mA/cm^2 and (c) 50 mA/cm^2.

Fig. 5 illustrates a photograph of the TiO_2 coating before and after treatment by MAO technology. The coating fabricated on the surface of Ti metal has a homogeneous structure. To further research the microstructure of the coating, the micro-surface morphology of the coating before and after MAO treatment was observed, and the results are shown in Fig. 6.

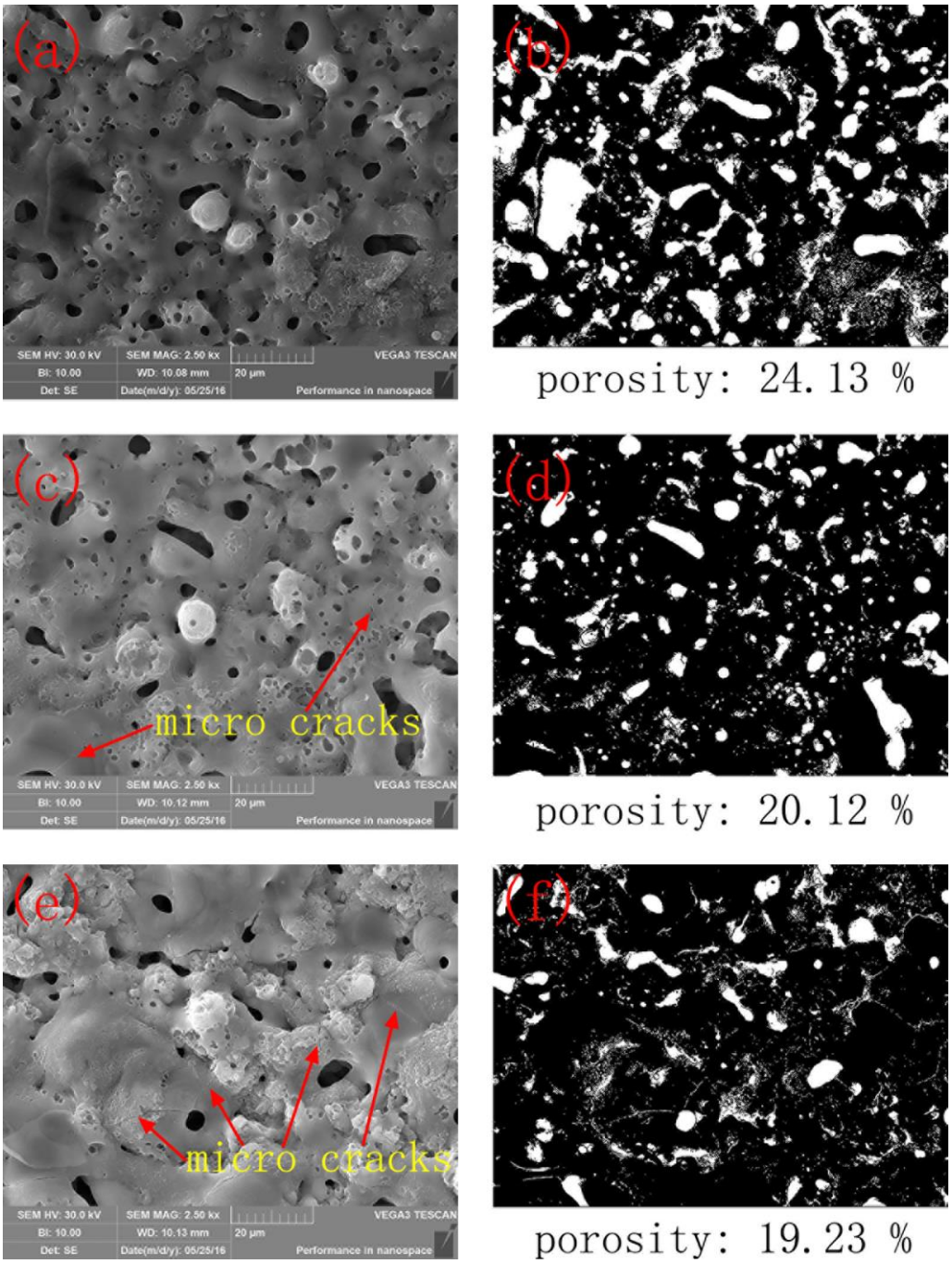

Figure 6. Micro-surface morphology (a, c, e) and porosity (b, d, f) of the TiO_2 coating treated by MAO technology in electrolytes containing 15 g/L Na_2SiO_3, 5 g/L $(NaPO_3)_6$, and 5 g/L KOH. The MAO procedure was conducted with a duty cycle of 10 %, a pulse frequency of 20 kHz for 15 min, and current densities of 10 mA/cm^2, 30 mA/cm^2 and 50 mA/cm^2.

It was reported that the quantity and size of the microcracks in the coating increased with increasing current density[39]. The results of Fig. 6 (a, c, e) proved this conclusion. Fig. 6 (b, d, f) shows that with increasing current density, the porosity of the coating decreased. The main reason was that after treatment by MAO technology, the pores of the anodic coating were sealed. The microcracks were caused by high temperature produced by plasma discharge, and the thermal stress increased with increasing current density, which led to an increase in the quantity and size of the microcracks. Because enhancing the porosity and reducing the size and quantity of microcracks are beneficial for increasing the specific surface area of the coating, to improve the activity of the photocatalyst, MAO should be carried out at a lower current density.

3.4 Absorbance of the coatings

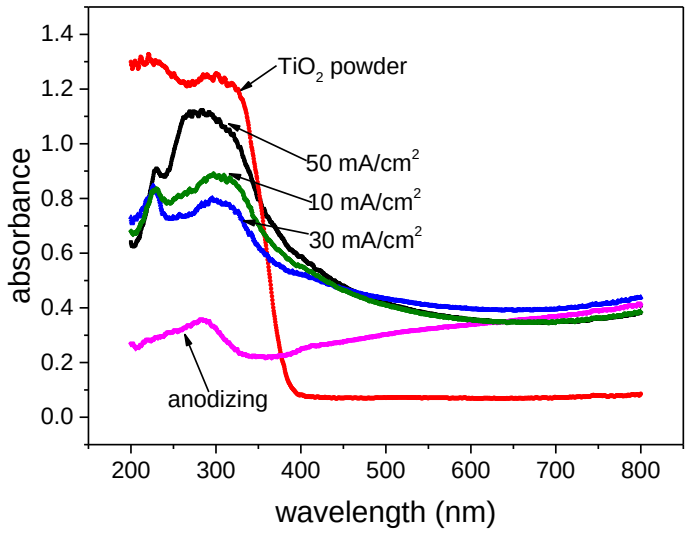

Figure 7. UV-vis absorbance of TiO_2 powder and anodic TiO_2 coating before and after MAO treatment in electrolytes containing 15 g/L Na_2SiO_3, 5 g/L $(NaPO_3)_6$, and 5 g/L KOH. The MAO procedure was conducted with a duty cycle of 10 %, a pulse frequency of 20 kHz for 15 min, and current densities of 10 mA/cm^2, 30 mA/cm^2 and 50 mA/cm^2.

Fig. 7 illustrates the UV-vis absorbance of the anodic TiO_2 coating before and after MAO treatment and compares it with the absorbance of TiO_2 powder. Fig. 7 shows that at a wavelength of 260 nm, the TiO_2 powder had a strong absorption peak, and the absorbance decreased rapidly with increasing wavelength[40]. While the anodic coating had a weak absorption peak at 260 nm, the absorbance was maintained and slowly increased as the wavelength increased. It was gratifying that after the coating was treated by MAO technology, there was a strong absorption peak at 260 nm, and the absorbance decreased slowly as the wavelength increased. The results proved that the TiO_2 coating had a wider absorption range than TiO_2 powder, which was beneficial for improving the activity of the photocatalyst.

3.5 Photocatalytic activity of the TiO_2 coatings

Fig. 8 illustrates the absorbance of the MO solution before and after 120 min of TiO_2 coating treatment. The untreated solution had two absorption peaks at 272 nm and 464 nm, representing the absorption of light caused by benzene and azo bonds, respectively. After it had been degraded by TiO_2 coating, the absorption peak at 272 nm disappeared, and the absorption peak at 464 nm decreased. When the current density was 30 mA/cm^2, both of the absorption peaks disappeared. When the current density was 30 mA/cm^2, the coating had better photocatalytic activity. In addition, there was a new absorption peak at 210 nm, which proved that an intermediate product was produced during the degradation process.

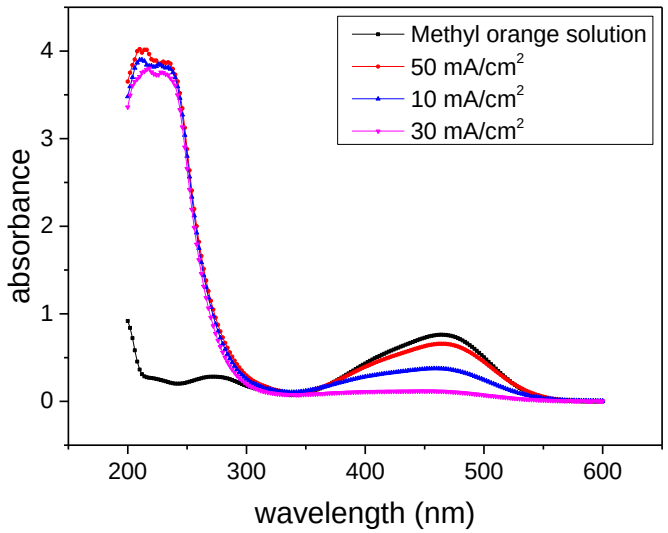

Figure 8. Absorbance of the MO solution before and after degradation by TiO_2 coating in an electrolyte containing 15 g/L Na_2SiO_3, 5 g/L $(NaPO_3)_6$, and 5 g/L KOH. The MAO procedure was conducted with a duty cycle of 10 %, a pulse frequency of 20 kHz for 15 min, and current densities of 10 mA/cm^2, 30 mA/cm^2 and 50 mA/cm^2.

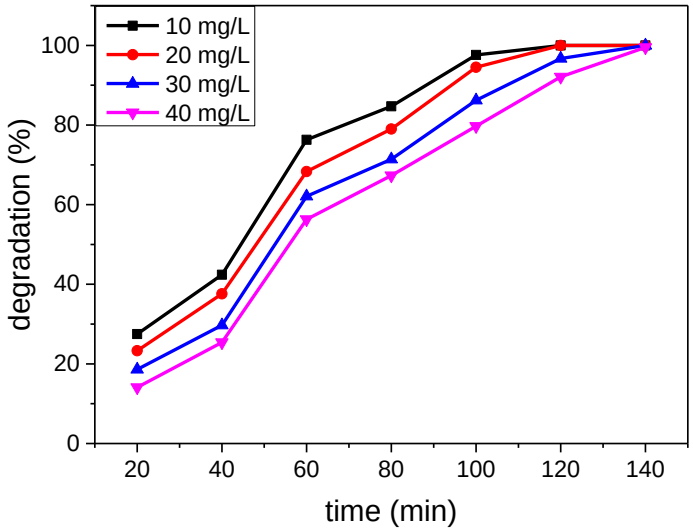

Figure 9. Degradation of MO at treatment times of 20 min, 40 min, 60 min, 80 min, 100 min, 120 min, and 140 min and concentrations of 10 mg/L, 20 mg/L, 30 mg/L and 40 mg/L

For the photocatalyst fabricated on the surface of titanium metal, it is difficult to evaluate the relationship between the contaminant concentration and the titanium oxide dosage; thus, a catalyst sample of the same size (20 × 20 × 1 mm^3) was used to degrade MO solutions with concentrations of 10 mg/L, 20 mg/L, 30 mg/L, and 40 mg/L. The influence of MO concentration and treatment time on the degradation was studied and is illustrated in Fig. 9. MO was easily degraded at a longer treatment times and lower concentrations, and similar results were reported in other studies[41]. It can also be seen that in the early stage of the photocatalytic reaction, the MO was degraded rapidly until the treatment time reached 60 min. When the treatment time reached 100 min and 120 min, the solutions with MO concentrations of 10 mg/L and 20 mg/L had degraded thoroughly, while it took 140 min to degrade the solutions with concentrations of 30 mg/L and 40 mg/L. The results proved that longer treatment times and lower MO concentrations were easier to degrade.

3.6 Stability of the coatings

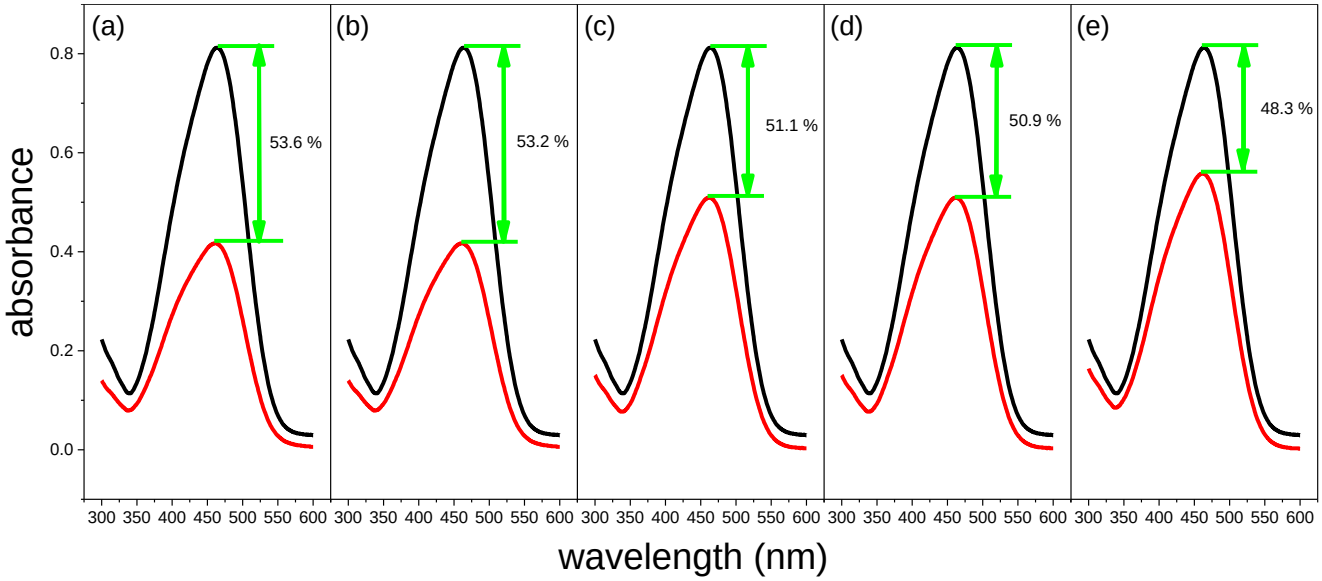

Figure 10. Influence of the photocatalyst used (a) 1, (b) 2, (c) 3, (d) 4 and (e) 5 times on the degradation of MO at a treatment time of 60 min and MO concentration of 20 mg/L

There is an absorption peak at 460 nm, and its intensity represents the degradation of MO solution. To reduce the operation error and instrument error, the absorbance of the MO was tested before and after treatment with the TiO_2 photocatalyst for 60 min, and the decrease in absorbance when the catalyst was used 1, 2, 3, 4, and 5 times was determined and is illustrated in Fig. 10. The specific activity of the catalyst was calculated and recorded in Table 1. Fig. 10 and Table 1 show that when the solution was treated with a new photocatalyst, the degradation of MO was 56.3 %, and with increasing reuse time, the degradation of MO decreased to 53.2 %, 51.1 %, 50.9 %, and 48.3 %, respectively. The specific activity decreased to 94.49 %, 90.76 %, 90.41 % and 85.80 %. The activity of the catalyst decreased

slowly with increasing use time, but after the catalyst was used 5 times, the specific activity exceeded 85 %, proving that the TiO_2 coating had better stability.

Table 1. The degradation of MO and the specific activity of the photocatalyst at a treatment time of 60 min and MO concentration of 20 mg/L after 1, 2, 3, 4, and 5 cycles

Use times	Degradation of MO (%)	Specific activity (%)
1	56.3	100
2	53.2	94.49
3	51.1	90.76
4	50.9	90.41
5	48.3	85.80

4. CONCLUSION

1) A TiO_2 coating was fabricated on the surface of Ti metal by combining anodizing and MAO technology. The pore size of the coating was observed by SEM, which proved that the pore size can be adjusted by using sulfuric-phosphoric acid as a mixed electrolyte in the anodizing process. The crystalline structure of the coating was characterized by XRD, which proved that its anatase and rutile ratio can be modified through the MAO process. The micro-surface of the coating was observed, and its porosity was calculated by ImageJ software, proving that the porosity of the coating can be improved. The suitable sulfuric-phosphoric acid concentrations were 110 g/L and 28.5 g/L in the anodizing process. The suitable current density was 30 mA/cm^2 during the MAO process.

2) The absorbance of the coating was measured and compared with that of TiO_2 powder by UV-vis spectroscopy, which proved that the coating had a wider absorption range. The photocatalytic activity of the coating on the MO solution was measured, which proved that prolonging the treatment time and decreasing the concentration of MO was helpful to increase the activity of the photocatalyst. In addition, even when the concentration of MO reached 40 mg/L, it could be degraded within 140 min. Additionally, the specific activity of the coating exceeded 85 % after it had been used 5 times.

References

1. Z. Irum, A. Muhammad, N. M. Anne, S. Tariq, U. Aman. *Chemosphere,* 273(2021):128545. 10.1016/J.CHEMOSPHERE.2020.128545
2. C. Y. Chun, T. T. Lung. *Mater. Chem. Phys.,* 267(2021):124700. 10.1016/J.MATCHEMPHYS.2021.124700
3. G. C. Liu, Z. H. Liu, L. Wang, K. Zhang, X. Y. Xie. *Chem. Phys. Lett.,* 771(2021):138496. 10.1016/j.cplett.2021.138496

4. K. S. J. Kumara, G. Krishnamurthy, P. Walmik, S. Naik, R. S. P. Rani, N. Naik. *Emergent Mater.,* 4(2021):457-468. 10.1007/S42247-021-00206-5
5. Z. Z. Hu, T. Xu, P. F. Liu, M. Oeser. *J. Cleaner Prod.,* 279(2021):123453. doi.org/10.1016/j.jclepro.2020.123453
6. X. X. Liu, X. Y. Yu, L. Sha, Y. Q. Wang, Z. Zhou, S. T. Zhang. *Chemosphere,* 270(2021):128609. doi.org/10.1016/j.chemosphere.2020.128609
7. J. S. Park, T. H. Lee, C. Y. Kim, S. A. Lee, M. J. Choi, H. Kim, W. J. Yang, J. Lim, H. W. Jang. *Appl. Catal. B,* 295(2021):120276. doi.org/10.1016/j.apcatb.2021.120276
8. S. Dmitry, S. Dmitry, K. Larisa, G. Evgeny, G. Alexey, K. Denis. *Colloids Surf. A,* 612(2021)5:125959. doi.org/10.1016/j.colsurfa.2020.125959
9. S. B. Nair, K. A. John, J. A. Joseph, S. Babu，V. K. Shinoj, S. K. Remillard, S. Shaji, R. R. Philip. *Phys. Status Solidi B,* 258(2020)4:2000441. 10.1002/pssb.202000441
10. Y. J. Lim, S. S. Lee. *Talanta open*, 228(2021):122233. 10.1016/J.TALANTA.2021.122233
11. D. K. Kanan, J. A. Keith, E. A. Carter. *ChemElectroChem*, 1(2014)2:407-415. 10.1002/celc.201300089
12. Y. A. Du, Y. W. Chen, J. L. Kuo. *Phys. Chem. Chem. Phys.,* 15(2013)45:19807-18. 10.1039/c3cp53091d
13. M. A. Rauf, S. S. Ashraf. *Chem. Eng. J.,* 151(2009)1:10-18. 10.1016/j.cej.2009.02.026
14. C. O'Rourke, A. Mills. *Chemosphere,* 271(2021):129847. doi.org/10.1016/j.chemosphere.2021.129847
15. W. Zhang, Y. Tian, H. L. He, L. Xu, W. Li, D. Y. Zhao. *Natl. Sci. Rev.,* 7(2020)11:1702-1725. 10.1093/nsr/nwaa021
16. K. Tamai, S. Hosokawa, H. Asakura, K. Teramura, T. Tanaka. *Catal. Today,* 332(2019):76-82. 10.1016/j.cattod.2018.07.045
17. K. Yang, Y. F. Zhang, Y. Li, P. Huang, X. Chen, W. X. Dai, X. Z. Fu. *Appl. Catal. B,* 183(2016):206-215. 10.1016/j.apcatb.2015.10.046
18. S. M. Kumar, M. M. Singh. *Opt. Mater.,* 109(2020):110309. 10.1016/J.OPTMAT.2020.110309
19. A. D. Gallo, M. R. Zierden, L. A. Profitt, K. E. Jones, C. P. Bonafide, A. M. V. Ann. *Metallomics,* 12(2020)1:8-11. 10.1039/C9MT00305C
20. X. Chen, Y. Huang, Y. H. Li, H. B. Li, G. J. Fan, R. Zhang, X. Y. Xu. *Mater. Lett.,* 293(2021):129709. doi.org/10.1016/j.matlet.2021.129709
21. J. X. Li, Y. Zeng, Y. H. Fang, N Chen, G P Du, A S Zhang. *Ceram. Int.,* 47 (2021) 7: 8859-8867. doi.org/10.1016/j.ceramint.2020.12.007
22. Y. Yao, L. X. Guan, Y. Ma, M. M. Yao. *J. Mater. Sci.:Mater. Electron.,* 28(2017)3:3013-3019. 10.1007/s10854-016-5887-1
23. H. Rafiee-Pour, M. Hamadanian, S. K. Koushali. *Appl. Surf. Sci.,* 363(2016):604-612. 10.1016/j.apsusc.2015.12.016
24. M. M. Zhang, J. Y. Chen, H. Li, C. R. Wang. *Rare Met.*, 40(2020)2:249-271. 10.1007/S12598-020-01499-X
25. J. Y. Zhang, H. J. Ai, M. Qi. *Surf. Coat. Technol.,* 228(2013)s1:202-205. doi.org/10.1016/j.surfcoat.2012.06.028
26. T. N. Trung, F. Z. Kamand, T. M. A. tahtamouni. *Appl. Surf. Sci.,* 505(2020): 144551. 10.1016/j.apsusc.2019.144551
27. R. Bahi, C. Nouveau, N. E. Beliardouh, C. E. Ramoul, S. Meddah, O. Ghelloudj. *Surf. Coat. Technol.,* 385(2020):125412. 10.1016/j.surfcoat.2020.125412
28. H. Lee, D. Y. Lee, M. H. Lee, B. Y. Kim, Y. S. Song. *J. Electroceram.,* 42(2019)3-4:124-128. 10.1007/s10832-018-0159-5
29. G. H. Jiang, X. Y. Zheng, Y. Wang, T. W. Li, X. K. Sun. *Powder Technol.,* 207(2011)1-3:465 469. 10.1016/j.powtec.2010.11.029
30. Q. Muhammad, Y. C. Li, B. Arne, W. Cuie. *Langmuir*, 37(2021)16:4984-4996.

doi.org/10.1021/acs.langmuir.1c00411
31. C. H. Liu, F. Wang, Y. Y. Qiu, Q. Liang, N. Mitsuzak, Z. D. Chen. *J. Photochem. Photobiol. A,* 353(2018):200-205. 10.1016/j.jphotochem.2017.11.022
32. Y. N. Zhang, Y. Han, L. Zhang. *J. Mater. Sci. Technol.,* 32(2016)9:930-936. 10.1016/j.jmst.2016.06.007
33. J. Ma, C. Z. Wang, C. L. Ban, C. Z. Chen, H. M. Zhang. *Vacuum,* 125(2016):48-55. 10.1016/j.vacuum.2015.12.005
34. F. Wang，H. Liu，Y. Wang，L. Meng，H. Bo. *Emerging Mater. Res.,* 4(2015)2:223-228. 10.1680/emr.15.00003
35. M. Mojtaba, R. Reza, H. N. Akbar, C. T. Mei, D. G. Li. *Mater. Des.,* 198(2021):109314. doi.org/10.1016/j.matdes.2020.109314
36. L. Zaraska, M. Jaskuła, G. D. Sulka. *Mater. Lett.,* 171(2016):315-318. 10.1016/j.matlet.2016.02.113
37. L. Özcan, T. Mutlu, S. Yurdakal. *Materials,* 11(2018)9:1715. 10.3390/ma11091715
38. M. Mumjitha, V. Raj. *J. Mech. Behav. Biomed.,* 46(2015):205-221. 10.1016/j.jmbbm.2015.02.006
39. V. Ezhilselvi, J. Nithin, J. N. Balaraju, S. Subramanian. *Surf. Coat. Technol.,* 28(2016):221-229. 10.1016/j.surfcoat.2016.01.040
40. W. C. Hung, Y. C. Chen, H Chu, T K Tseng. *Appl. Surf. Sci.,* 255(2008)5:2205-2213. 10.1016/j.apsusc.2008.07.079
41. M. M. Wang, Y. K. Cu, H. Y. Cao, P. Wei, C. Chen, X. Y. Li, J. Xu, G. P. Sheng. *Appl. Catal. B,*282(2021):119585. 10.1016/J.APCATB.2020.119585